Available online at www.sciencedirect.com
ScienceDirect
Cement and Concrete Research 38 (2008) 27–39
Cement and Concrete Research

# Modeling of frost salt scaling

Oğuzhan Çopuroğlu *, Erik Schlangen

*Delft University of Technology, Faculty of Civil Engineering and Geosciences, Micromechanics Laboratory (MICROLAB), Delft, The Netherlands*

Received 8 February 2007; accepted 3 September 2007

**Abstract**

This paper discusses the numerical modeling of deterioration in cement-based materials due to frost salt scaling (FSS). Several aspects of FSS are investigated such as carbonation, microstructure, mechanical properties and testing conditions. Mainly blast-furnace slag cement (henceforth *slag cement*) systems are of interest in this paper since several reports have been indicated that cementitious materials bearing slag-rich cement are critically vulnerable under combined attack of frost and de-icing salts.

In the first part, the paper deals with the effect of carbonation on the micromechanical properties and FSS resistance of 1-year-old slag cement and ordinary Portland cement pastes with W/C 0.45. The micromechanical properties were evaluated by the nano-indentation technique and the results are used to evaluate the behavior of these pastes under frost salt attack. FSS damage on the paste samples is modeled according to the *glue-spall* theory with the aid of Delft Lattice Model. Additionally, the carbonated cement paste microstructures are characterized by ESEM/BSE.

In the second part, parameters that are varied in the investigation are the salt concentration in the external water layer and ice-layer thickness on the surface. Again the lattice type model is used to simulate the mechanism in which the material structure is implemented using digital images of the real material. Both experiments and the simulation with the model show that the amount of scaling increases with increasing thickness of the ice layer on the surface. Furthermore it is shown that with the model the well known pessimum effect for salt concentration in the water (which causes maximum damage at 3% salt) can be reproduced.

The outcome of the model indicates that *glue-spall* theory can successfully explain FSS.


*Keywords:* Frost salt scaling; Freezing and thawing (C); Micromechanics (C); Modeling (E); Granulated blast-furnace slag (D)

## 1. Technical background

The modeling of FSS has been a difficult issue due to its complex physical and chemical mechanisms [1]. Plain frost action has attracted relatively more attention and thanks to its less complicated mechanism, we increased our knowledge during the past few decades. The works of Powers, Litvan, Pigeon, Marchand, Setzer [2–5], and many other researchers have drawn the frame of the issue substantially. Unfortunately, similar arguments could not be made for frost salt attack. There have been a number of questions, which could not be answered by a single theory [6]. Due to having insufficient knowledge about the phenomenon, modeling attempts have been restricted to black-box type [7]. However, recently an interesting theoretical explanation of the mechanism of frost salt attack was introduced by Valenza and Scherer [8,9]. The researchers proposed a mechanism called *glue-spall*. According to this theory the cracking of the ice/brine layer is the origin of FSS. They put forward a theoretical explanation for the greater damage of pessimum salt concentration under frost which has been known as a mystery so far. The principle idea is that following the ice formation on top of the concrete surface, ice starts to shrink due to further cooling. The shrinkage creates tensile stresses in the ice and causes three consequences depending on the solute concentration of the liquid. These are:

1. Weak salt concentration (*i.e.* 0.1%): Due to the ice formation and further cooling of the ice, the exerted tensile stress cannot exceed the tensile strength of ice; hence no cracking occurs (in ice and concrete).
2. Pessimum salt concentration (1–3%): Due to the ice formation and further cooling of the ice, the exerted tensile

* Corresponding author.
*E-mail address:* o.copuroglu@citg.tudelft.nl (O. Çopuroğlu).

0008-8846/$ - see front matter © 2007 Elsevier Ltd. All rights reserved.
doi:10.1016/j.cemconres.2007.09.003

stress exceeds the tensile strength of ice and breaks the ice, which triggers surface scaling.
3. Strong salt concentration (10–20%): In this case the ice layer is too soft to exert enough stress to the underlying cementitious material, hence only the ice cracks and no scaling occurs.

Therefore, tensile strength of a cement-based material seems to be an essential indicator concerning the FSS resistance of cement-based materials. The study of the *glue-spall* theory has shown that scaling occurs due to the cracking of the external ice layer and consequent generation of tensile stress on the surface layer. However, simply considering the global tensile strength of a cementitious material may not be an appropriate approach to the problem since the tensile strength highly depends on the strength of the weakest link in the specimen under tensile stress (see Fig. 1a). In case of FSS, the picture is a bit more complex where the micromechanical properties of the phases in different locations determine the scaling resistance throughout the material surface (Fig. 1b). Therefore assessment of local micromechanical properties seems to be much more crucial than evaluation of global tensile strength in order to predict the FSS resistance of a particular material.

For the measurement of local micromechanical properties, depth-sensing nano-indentation has been shown to provide a useful tool, especially for measuring hardness and elastic modulus of local phases/materials on the submicron scale [10]. This has been achieved principally through the development of instruments capable of continuously measuring load and displacement throughout an indentation. With this method and high precision instrument, the mechanical properties can be determined directly from indentation load and displacement measurements without the need to image the indent impression. Details of such a technique, which was used successfully to study properties of the interfacial transition zone (ITZ) in practical concrete and individual phases in cement paste, have been given elsewhere [11–13].

The FSS modeling is very much restricted by the lack of data concerning the mechanical properties (*i.e. E*-modulus, strength) of the micromaterials and more specifically, by the lack of data obtained *in situ*. Very little information is found on the micromechanical properties of cementitious materials in the literature [14]. Constantinides and Ulm [13] reported the elastic modulus of C–S–H, decalcified C–S–H, calcium hydroxide and unhydrated clinker ranging between 19.5 and 31.8 GPa, 2.2 and 13.2 GPa, 33 and 43 GPa and over 100 GPa, respectively. The tensile strength cannot be measured directly but could be estimated from the elastic modulus of the phases.

Furthermore, the properties of the above mentioned cement paste phases appear to be influenced by different cement types as well as environmental conditions, which affects various aspects of cement-based materials, including FSS. It is reported that slag-rich cement concrete and ordinary Portland cement (OPC) concrete perform differently when subjected to carbonation [15]. While carbonation leads to a slight densification of the microstructure in OPC concrete, in slag cement concrete the microstructure becomes coarser. The percentage of capillary pores increases with carbonation in slag cement concrete, while in the case of OPC it decreases. More recent electron microscopy and mercury intrusion porosimetry studies have further confirmed that carbonation causes remarkable coarsening of the slag-rich cement paste microstructure [16,17]. The visual findings from the electron microscopy imply that there could be a significant decrease in tensile strength of the slag cement paste which could be the reason for increased vulnerability of the concrete surface against the attack of frost and de-icing salts.

Among the influencing parameters, a high priority has to be given to carbonation since the mechanical properties (and indirectly FSS performance) of a cement-based material can be significantly influenced by this environmental issue. Only a small number of researchers reported the strength sensitivity of slag cement-based materials to carbonation [18–20]. Manns and Wesche investigated the effect of carbonation on the flexural strength of the high-slag (82% slag m/m) cement mortars with W/C 0.50. They concluded that the higher the degree of carbonation, the lower the rupture modulus of high-slag cement mortars. They also observed that flexural strength of OPC and low-slag cement mortars were not negatively affected by the carbonation [21].

This paper discusses the numerical and visual modeling of the FSS phenomenon according to the *glue-spall* theory. Various experimental results are used as an input for the model and the validation of the model is also discussed with the

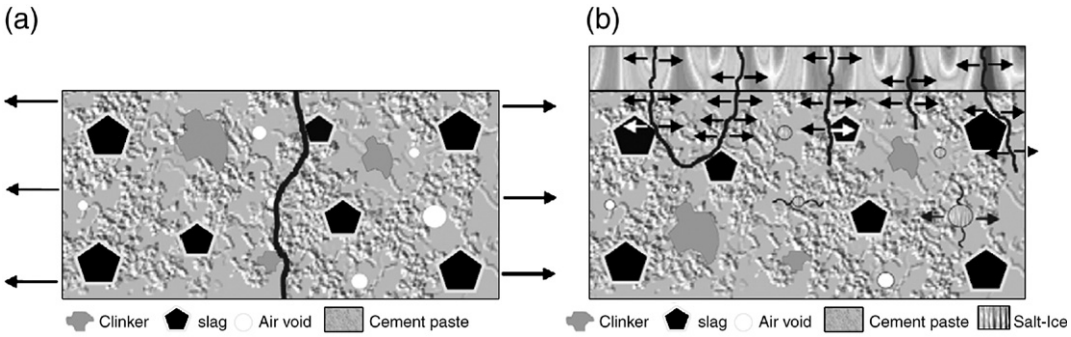


Fig. 1. Schematic description of a cement paste under global tensile stress and of the cracks induced by the cracking of external ice layer.

laboratory findings. The aim of the study is to investigate whether or not the *glue-spall* theory can explain FSS phenomenon and to put forward the effectiveness of Delft Lattice Model as a computational tool.

## 2. Experimental data

### 2.1. Experimental details for "the effect of carbonation" study

The effect of carbonation on the micromechanical properties of CEM III/B 42,5 N HSR LH (67% slag m/m) and CEM I 32,5 R pastes with W/C ratio 0.45 were investigated (see Table 1 for the cement properties). After the preparation, the paste specimens were kept at 20 °C, in 95% R.H. environment for 1 year. At the end of the curing period, half of the specimens from each cement paste series were carbonated in 3% $CO_2$/20 °C/55% R.H. chamber for 2 weeks. After the carbonation period, the specimens were ground with grade #1200 and #4000 sand papers and polished with 6 μm, 3 μm, 1 μm and 0.25 μm polishing paste on a lapping table. Finally, the specimens were soaked into the ultrasonic bath to remove the polishing paste and other particles away from the surface. The quality of the indentation surface was checked by optical microscopy. A summary of the curing regimes and the cement types are given in Table 2).

Polished specimens were investigated using a Philips XL30 environmental scanning electron microscope (ESEM). The instrument was operated at 15 kV accelerating voltage, beam current 20 mA, 0.3 Torr pressure and at approximately 10 mm working distance for image acquisition.

The nano-indentation apparatus used was Nanoindenter XP with a load range of 0–10 N (MTS Systems Corporation). The resolutions for load and displacement measurement were 50 nN and 0.04 nm, respectively. A diamond Berkovich tip was used for the test. In this study all testing was programmed in such a way that the loading started when the indenter came into contact with the test surface and the load was maintained for 30 s at the pre-specified maximum value before unloading. Multiple loading–unloading cycles were applied at each test point, so as to allow assessment of the micromechanical properties at different length scales to be made. The specimen elastic modulus can be calculated using the following formula [10]:

$$1/E_r = \left(1-\upsilon_s^2\right)/E_s + \left(1-\upsilon_i^2\right)/E_i \quad (1)$$

where, $E_r$ is the reduced elastic modulus which can be obtained from the slope of an unloading curve (Fig. 2) of an indentation, $\upsilon_s$ is the Poisson's ratio of the sample, $\upsilon_i$, is the Poisson's ratio of the indenter (0.07), $E_s$ is the Young's modulus of the sample and $E_i$ is the Young's modulus of the indenter (1141 GPa) [10].

Table 1
Physical and chemical properties of CEM I 32,5 R and CEM III/B 42.5 N HSR LH

| Chemical | | Physical | |
|---|---|---|---|
| | | Compressive strength of standard mortars | |
| *CEM I 32,5 R* | | | |
| CaO, % | 63.9% | 2 days | 22.0 MPa |
| $SO_3$, % | 2.68% | 7 days | 36.0 MPa |
| $SiO_2$, % | 20.6% | 28 days | 49.0 MPa |
| $Al_2O_3$, % | 5.01% | Blaine | 285 $m^2$/kg |
| *CEM III/B 42,5 N HSR LH* | | | |
| CaO | 44.9% | 2 days | 11.9 MPa |
| $SO_3$ | 3.38% | 7 days | 34.1 MPa |
| $SiO_2$ | 27.7% | 28 days | 53.5 MPa |
| $Al_2O_3$ | 12.0% | Blaine | 376 $m^2$/kg |

Table 2
Curing regimes of the paste specimens used in the nano-indentation study

| Paste (W/C 0.45) | Curing | Carbonation |
|---|---|---|
| CEM I 32,5 R | 1 year at 20 °C, 95% | 2 weeks in 3% $CO_2$ at 20 °C, 55% R.H. |
| CEM I 32,5 R | 1 year at 20 °C, 95% | – |
| CEM III/B 42,5 N HSR LH | 1 year at 20 °C, 95% | 2 weeks in 3% $CO_2$ at 20 °C, 55% R.H. |
| CEM III/B 42,5 N HSR LH | 1 year at 20 °C, 95% | – |

### 2.2. Experimental details for "effect of testing parameters" study

Two testing parameters were of interest in this study; effect of external ice-layer thickness (EXP1) and effect of salt concentration on FSS (EXP2).

A standard (W/C 0.50) mortar mixture with CEM III/B 42,5 N HSR LH (see Table 1) was prepared according to EN 196 [22]. The reason for using mortar specimens (instead of concrete) in this study was to minimize the surface heterogeneity and the specimen-to-specimen variation. The mixture was then poured into the 18 × 13.5 cm cylindrical plastic moulds to the thickness of 35 mm. Then the buckets were vibrated identically for 10 s. Finally polyethylene sheets with the diameter of 18 cm were placed on the top surface. Air pores on the specimen surfaces were scraped out by a plastic spatula to obtain a reasonably flat testing surface. During the testing period, the buckets were closed by plastic lids in order to prevent evaporation. Only 1 specimen was tested per solution strength or ice-layer thickness.

The specimens were cured in water for 1 week and exposed to 3% $CO_2$ accelerated carbonation at 55% R.H. for an additional 1 week. The aim was to further weaken the surface in order to achieve magnified damage which would make the evaluation and the comparison of the scaling results easier for various ice thicknesses. Finally, prior to the scaling test, the samples were saturated with 3% NaCl solution for 2 weeks for EXP1 and the corresponding salt solutions (0%, 1%, 3%, 7% and 10%) for EXP2.

The effect of four different ice thicknesses, 1 mm, 3 mm, 5 mm and 10 mm and the effect of five external salt solution strengths, 0%, 1%, 3%, 7%, and 12%, were investigated. The depth of external salt solution was 3 mm in the latter experiment. The freezing–thawing cycles of 17 ± 1 h freezing at −20 ± 2 °C and 7 ± 1 h thawing at 20 ± 2 °C were maintained. 3 cycles were

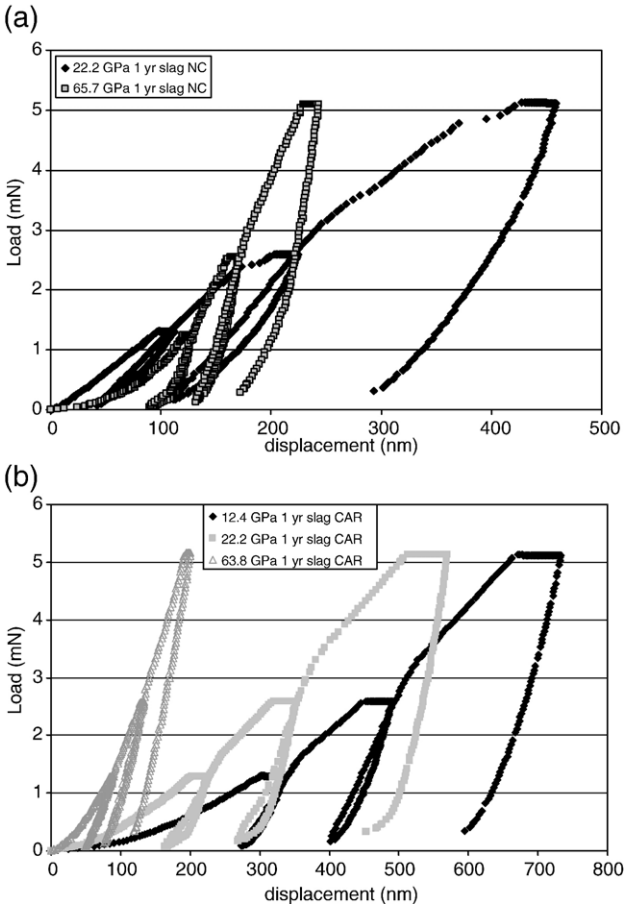


Fig. 2. Typical load–displacement curves of 1-year-old (a) non-carbonated and (b) carbonated slag cement paste.

completed for each series and scaled material was collected by filtration after each cycle. Scaled materials were then placed in the stove at 110 °C and weighed after 24 h of drying.

The testing was stopped in EXP1 and EXP2 after 3 freezing–thawing cycles because the surface of the specimens became seriously damaged and maintaining the test liquid at the desired thickness throughout the whole surface was no longer possible.

## 3. Nano-indentation test results and ESEM observations

The typical nano-indentation results of the 1-year-old non-carbonated and carbonated slag cement pastes are presented in Fig. 2a and b. In non-carbonated slag paste two distinct phases were identified. In view of the findings from the literature, those are regarded mainly as the micromechanical values for the hydrated cement paste and presumably the unreacted slag/clinker particles.

The effect of carbonation on the microstructure of slag cement paste was also characterized by the nano-indentation. In comparison to the non-carbonated slag cement paste a different phase was identified. This new phase had a lower elastic modulus than the lower limit for C–S–H as suggested by Constantinides and Ulm [13] and showed similar characteristics to Ca-leached (or decalcified) C–S–H, ranging between 12.1 and 19.5 GPa.

The collective nano-indentation results of carbonated and non-carbonated slag cement pastes are presented in Fig. 3a in the form of a histogram. The results represent up to 60 indentations per sample. It can be clearly seen that carbonation causes significant reduction of the elasticity modulus in the 20–45 GPa zone where it corresponds to matrix, and a dramatic increase of the zones having elasticity modulus of 0–20 GPa.

The earlier findings [16,17] in the electron microscopy and mercury intrusion porosimetry investigations are supported by the results presented in this experimental study. It was observed that carbonation shrinkage significantly reduces the elastic modulus and most probably the tensile strength of the carbonated slag cement paste and this inevitably decreases the FSS resistance.

Additional nano-indentation tests were also carried out on 1-year-old carbonated and non-carbonated OPC pastes (W/C = 0.45). The results are summarized in Fig. 3b. It was seen that carbonation is rather favorable with respect to the elastic modulus and tensile strength of OPC paste. The histogram of the nano-indentation results in Fig. 3b shows that the OPC paste possesses 40% of the total phases in 0–20 GPa zone. This is reduced to approximately 10% after the carbonation. The

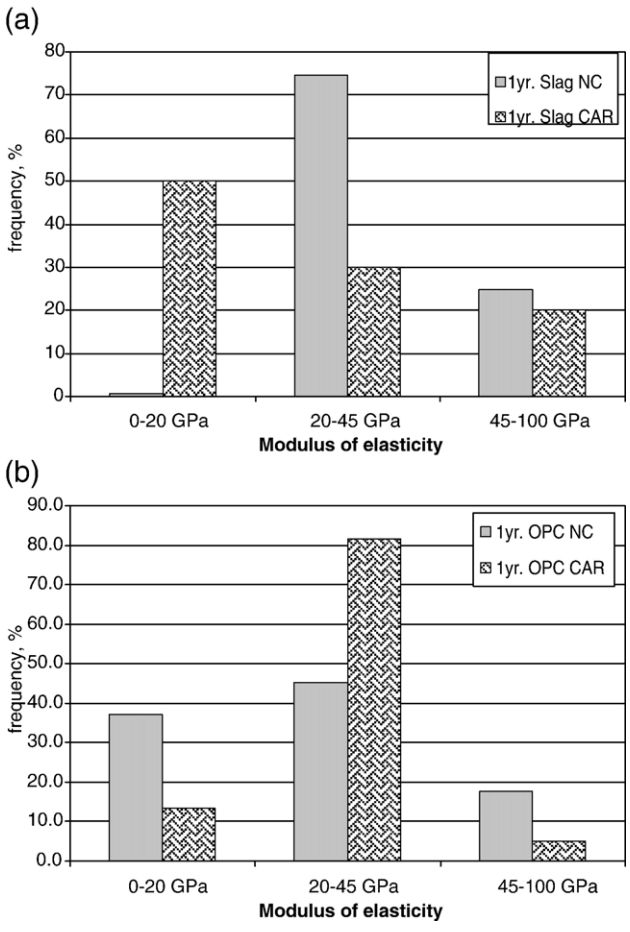


Fig. 3. Summary of (a) the 1-year-old slag cement paste and (b) OPC paste (W/C 0.45) nano-indentation test results. NC: non-carbonated, CAR: carbonated.

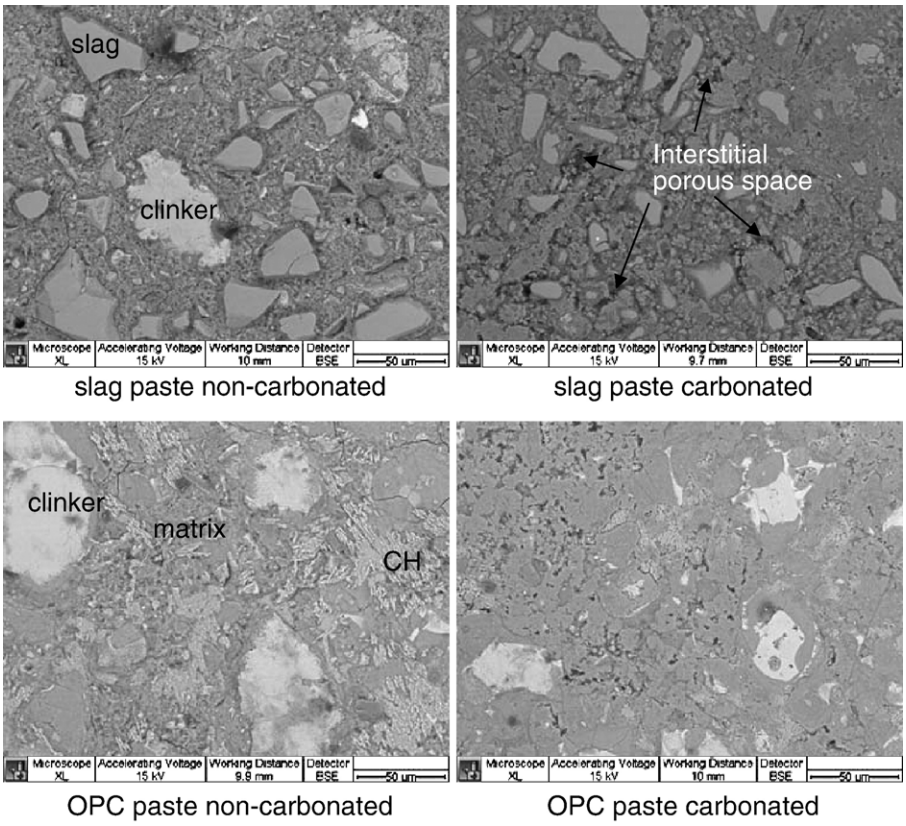


Fig. 4. Photomicrographs of 1-year-old high-slag and OPC pastes in non-carbonated and carbonated conditions (W/C = 0.45).

carbonation led to a 100% increase of the amount of phases in the 20–45 GPa zone compared to the non-carbonated OPC paste. Overall elastic modulus and tensile strength are increased significantly and consequently a resistant microstructure is achieved by carbonation.

The microstructure of the cement pastes before and after the carbonation can be seen in Fig. 4. Carbonated slag cement paste microstructure demonstrates significant coarsening while OPC paste becomes relatively denser by the carbonation of portlandite crystals. Disappearance of the portlandite by carbonation is quite visible in the ESEM/BSE microphotographs in Fig. 4 (lower row).

## 4. Effect of testing parameters on FSS

### 4.1. Ice-layer thickness

As presented in Fig. 5, the experimental study revealed the effect of ice thickness on the scaling of the underlying cementitious material. It was clearly observed that for an identical freezing–thawing cycle, salt concentration of freezing liquid and the material properties, higher thickness of ice generates more damage on the material surface. 1 mm of initial depth of freezing liquid gave 74 g (1.3 kg/m$^2$) of cumulative mass scaling after 3 cycles while 10 mm caused the scaling of 103 g (1.8 kg/m$^2$). It should be stressed that a 9 mm increase in the initial freezing liquid thickness causes 40% more mass scaling after only three freezing–thawing cycles.

It was observed that 10 mm ice-layer thickness generates mass scaling with significant number of larger flakes in comparison to the one with 1 mm ice thickness. The typical scaled-off particles can be seen in Fig. 6.

### 4.2. Pessimum effect

The experimental results seconded the results provided by the previous researchers [23]. In Fig. 7 the surface scaling after three freezing–thawing cycles from the experimental study is provided.

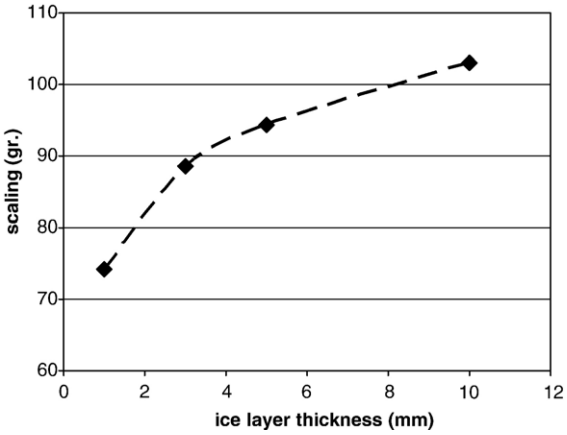


Fig. 5. Cumulative mass scaling of the identical samples with various ice-layer thicknesses (after 3 freezing–thawing cycles).

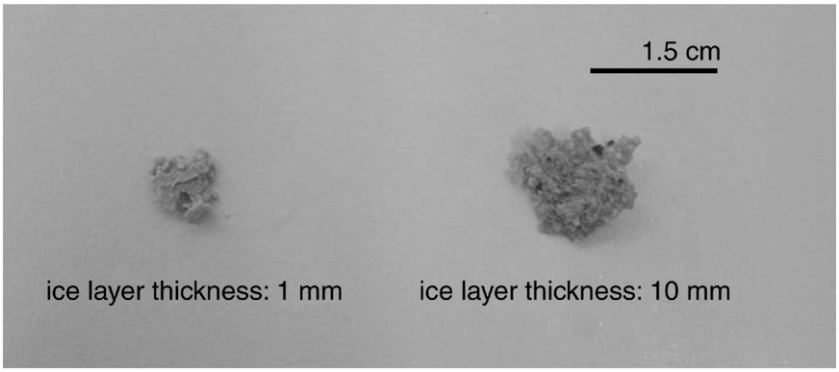


Fig. 6. Typical scaled-off flakes from the mortar specimens having 1 mm (left) and 10 mm (right) thick ice layers on top.

It can be noticed that indeed 3% NaCl concentration causes the severest damage compared to the other concentrations.

## 5. Modeling aspects and simulations

### 5.1. Principles of the Delft Lattice Model

Heterogeneous materials have complicated fracture mechanisms, which are related to their microstructure. The use of linear elastic fracture mechanics to analytically describe these mechanisms is very hard, since fracture patterns consist of a main crack, with various branches, secondary cracks and microcracks. Lattice type models are used by theoretical physicists [24] to model fracture mechanisms in various materials. To model concrete fracture these models were introduced by Schlangen and van Mier [25]. Lattice models are now used quite a lot to model concrete crack patterns, mainly because the simulated cracks are very realistic and resemble to a great detail the cracks observed in laboratory tests and in practice [25–29]. In these models a material is discretized as a lattice consisting of small beam (or spring) elements that transfer forces, as can be seen in Fig. 8.

The meshes used in this paper are 2D regular triangular meshes. Other options like random meshes are sometimes preferable if the crack pattern precision is of concern, see [26]. Each of the beams in the lattice can transfer, in general, normal force ($F$), shear force ($Q$) and bending moment ($M$). The relation among these forces and corresponding displacements for the endpoints (i and j in Fig. 8) of a beam can be expressed as follows:

$$F_i = \frac{EA}{l}\left(u_i - u_j\right) \tag{2}$$

$$Q_i = \frac{12EI}{l^3}\left(v_i - v_j\right) - \frac{6EI}{l^2}\left(\phi_i - \phi_j\right) \tag{3}$$

$$M_i = \frac{6EI}{l^2}\left(v_j - v_i\right) + \frac{4EI}{l}\left(\phi_i - \frac{\phi_j}{2}\right) \tag{4}$$

in which $E$ is Young's modulus, $l$ is the length, $A$ is the cross-sectional area and $I$ is the moment of inertia of a beam element, $(u, v)$ are the translational displacements and $\phi$ is the nodal rotation.

For a lattice with a regular geometry, the quantities $E$, $A$, $l$ and $I$ are in principle, equal for all elements. However, these parameters can be varied, either element by element or according to a superimposed microstructure, in order to implement heterogeneity.

To construct the system of equations for the complete lattice, each element matrix has to be multiplied by the appropriate rotation matrix and positioned correctly in the system. The final set of equations for the system is of the form:

$$b = Ax \tag{5}$$

in which $b$ is the force vector, $S$ is the stiffness matrix and $x$ is the displacement vector. If there are $N$ nodes in the system, then $b$ and $x$ are of length $3N$ and in general a $3N \times 3N$ matrix.

When solving the set of linear elastic equations for a lattice under an applied load, the load vector and stiffness matrix are known and the displacement vector is to be determined by solving Eq. (5). One method to solve the set of equations is to use a direct solver which finds the inverse of $S$ by Gaussian elimination. In the simulations presented in this paper the displacement vector $x$ is solved iteratively by minimizing the functional $G$, which has the dimensions of energy,

$$G = 0.5xSx - bx. \tag{6}$$

The loading in case of the simulation of FSS is the shrinkage of the ice. The elements in the mesh representing the ice

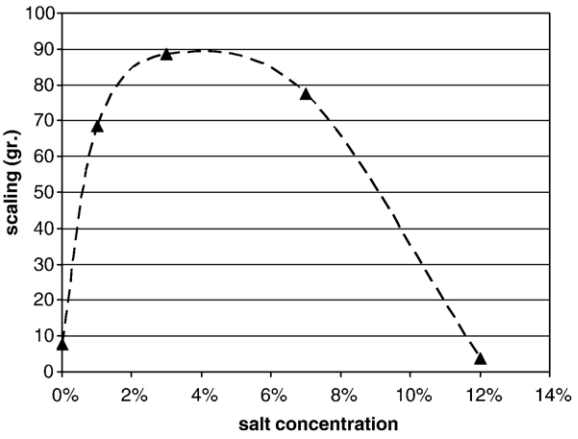


Fig. 7. Effect of NaCl concentration on the FSS of carbonated slag cement mortars.

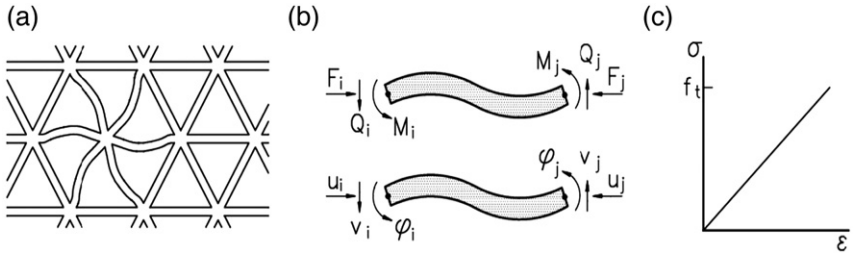


Fig. 8. (a) Lattice of beams, (b) definition of forces and degrees of freedom, (c) stress strain relation of beam element.

undergo a pre-defined dilation which is transferred to prescribed nodal forces in the nodes of the elements [30]. The simulation of fracture proceeds as follows. A linear elastic analysis of the lattice is performed. If the stress in one of the beams exceeds the material strength this beam virtually breaks and is removed from the lattice. Then the deformations of all the nodes and the stresses in all the beams are recalculated and compared again with their strength, which may result in the next beam to break.

### 5.2. Modeling basics of FSS mechanism

According to the *glue-spall* theory, a layer of ice forms on top of the material, then the ice shrinks and cracks as the temperature drops. Due to the cracks in the ice, shear stresses are created which cause the concrete to crack and pieces of material to scale off. This is modeled with the lattice model as shown in Fig. 9. An arbitrary layer of 3 mm ice on top of 12 mm mortar is modeled. In the horizontal direction periodic boundary conditions are assumed. At the bottom and at the top the nodes are free. The properties in Table 3 are used.

The analysis is performed linear elastic. It is assumed that the temperature drops −20 °C and that the difference in thermal dilation between the concrete and the ice is $4\times10^{-5}$. In the analysis actually no relaxation of the stresses is used. The first crack in the ice, however, starts already at 10% of the applied strain and the ice cracks through at 13.5% of the applied strain, or in other words at a temperature change of only −2.7 °C. This is somewhat less than the linear elastic calculation in [8,9], where a temperature decrease to −4 °C would lead to cracking. However in case the ice layer is placed on a heterogeneous microstructure the restraining of the ice is not uniform. Due to variations in stiffness of the supporting microstructure, stress concentrations in the uniform ice will appear which results in earlier cracking than the linear elastic calculation gives.

In practice a lot of the linear elastic stress will disappear due to relaxation of the ice and also of the cement-based material under it. This is also described by Valenza and Scherer [8,9]. Due to this relaxation the generated stresses for the complete temperature drop of −20 °C will not be enough to crack pure ice, but will be enough to crack brine ice, as will be further discussed in this paper. The crack continues in the mortar and kinks at a certain distance inside the material. Afterwards it continues until it hits the ice again, and a second crack in the ice is formed. Further continuation of the simulation would create another crack in the ice at another location, and the mechanism would repeat again. Of course also here the mechanism is influenced by the choice of local material properties and relaxation of stresses.

### 5.3. Modeling FSS — OPC vs. slag cement

In this study, the micromechanical values of 1-year-old high-slag cement and OPC pastes were used to construct the microstructure of carbonated and non-carbonated pastes. The micromechanical values were obtained from nano-indentation as described in Section 3. The built-up structures were used in

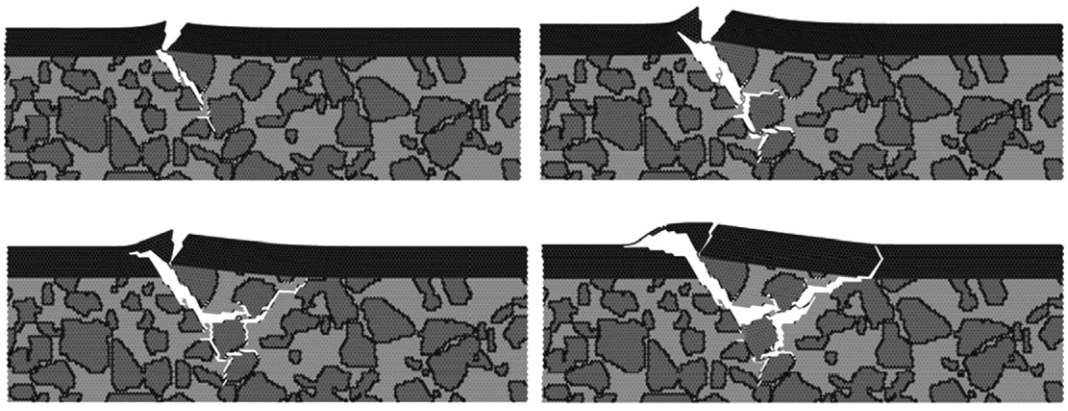

Fig. 9. Simulation of a FSS action by Delft Lattice Model.

Table 3
Material properties used in lattice simulations of concrete with ice layer

| Material | *E*-modulus [GPa] | Tensile strength [MPa] |
|---|---|---|
| Aggregate | 70 | 10 |
| Matrix | 25 | 4 |
| Interface | 10 | 1 |
| Ice | 10 | 2.5 |

the numerical model to evaluate the FSS performances under the identical frost loading conditions. The idea was to study the effect of carbonation on the high-slag and OPC pastes microstructure and its effect on the FSS. Until now, the dissimilar FSS performances of high-slag cement and OPC pastes (and concretes) could not be explained thoroughly [31]. With the help of the new numerical model and the *glue-spall* theory, the phenomenon behind this dissimilarity can be further elaborated and understood.

The acquisition of BSE images of the paste samples to be modeled was considered as a perfect starting point. The threshold of the BSE images provides a more realistic model than randomly distributing the paste phases (Fig. 10). The next step is to assign the volumetric proportion of the unreacted solids/particles (USP), hydrates in the matrix (HM) and porous interstitial space (carbonated weak zones, PIS) into the images (Fig. 10b,c). Increase or decrease of the PIS is calculated according to the observations in the nano-indentation test (Fig. 3). The weak zones are generally observed around the unreacted particles in the ESEM studies [16]. In the images the PIS is increased or decreased by dilating or eroding the particles. An arbitrary layer of 25 μm ice on top of 190 μm paste is considered and the properties in Table 4 are used for the phases. In this study, an estimate of 1/10,000 *E* was assumed to take a reasonable approximation for the tensile strength values of the cement paste phases.

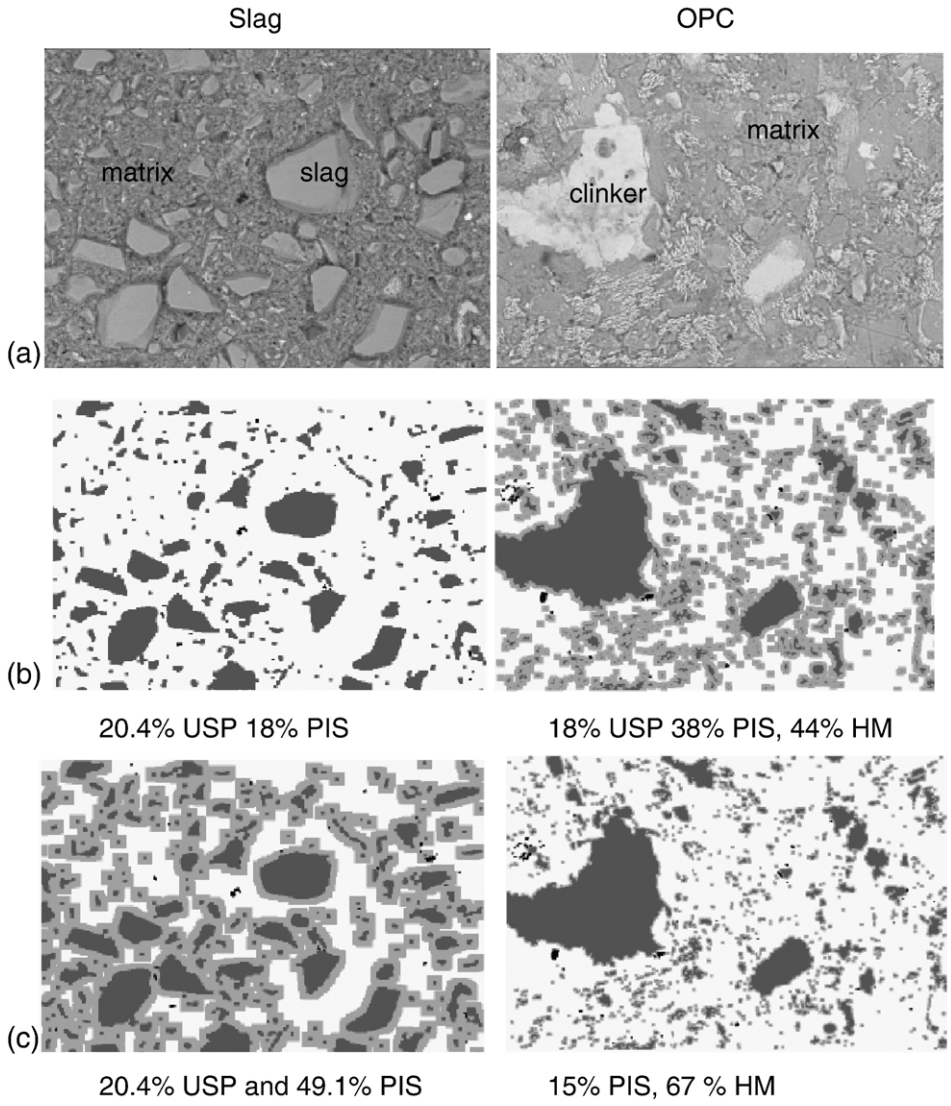


Fig. 10. (a) ESEM/BSE microphotographs of non-carbonated slag cement and OPC pastes. (b) Threshold images of non-carbonated pastes (c) threshold and modified images of carbonated pastes according to the nano-indentation test results.

Table 4
Micromechanical properties of the cement paste constituents (as used in the numerical model)

| Phases | Elasticity modulus[a] [MPa] | Tensile strength [MPa] |
|---|---|---|
| Salt–ice | 10,000 | 2.5 |
| C–S–H (matrix), HM | 32,500 | 3.25 |
| Decalcified C–S–H, PIS | 10,000 | 1.0 |
| Slag/clinker, USP | 72,500 | 7.25 |

[a] Average values from the three zones in Fig. 2.

In Fig. 11 the modeled scaling performances of OPC and slag cement pastes are presented. Carbonated slag cement paste exhibits the greatest damage of all. Non-carbonated slag paste had a good resistance while non-carbonated OPC showed inferior performance compared to carbonated OPC paste. It should be noted that the results illustrate comparative performances of the pastes. The effect of ice expansion in the capillary porosity is neglected in the modeling, so the FSS on the paste samples are generated purely by the *glue-spall* action.

### 5.4. Modeling experimental parameters — ice-layer thickness

In this model, the micromechanical parameters in Table 3 were used. Note that these values differ from the parameters obtained by nano-indentation as used in the previous section. The intention was only to model in a qualitative way the effect of ice thickness as well as simulating the damage pattern occurring under the effect of different ice thicknesses. It should be noted that here the mechanical properties of ice represent plain ice. However the damage pattern depends significantly on the mechanical properties of the material. Hence, the aim is to

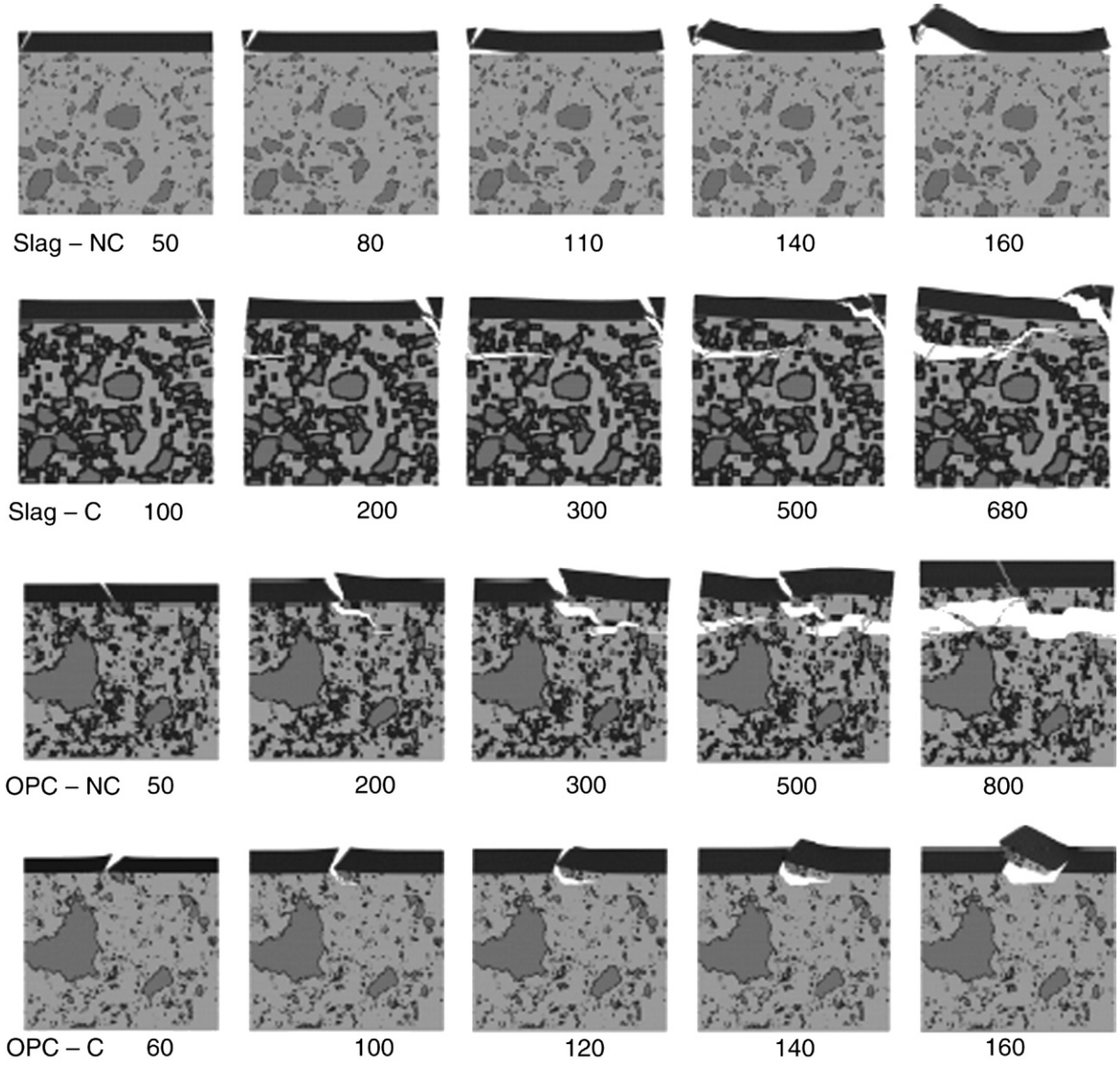


Fig. 11. Modeling of FSS performances of slag cement paste and OPC paste in carbonated and non-carbonated conditions. NC: non-carbonated, C: carbonated. The numbers denote the number of cracked beam elements in the mash.

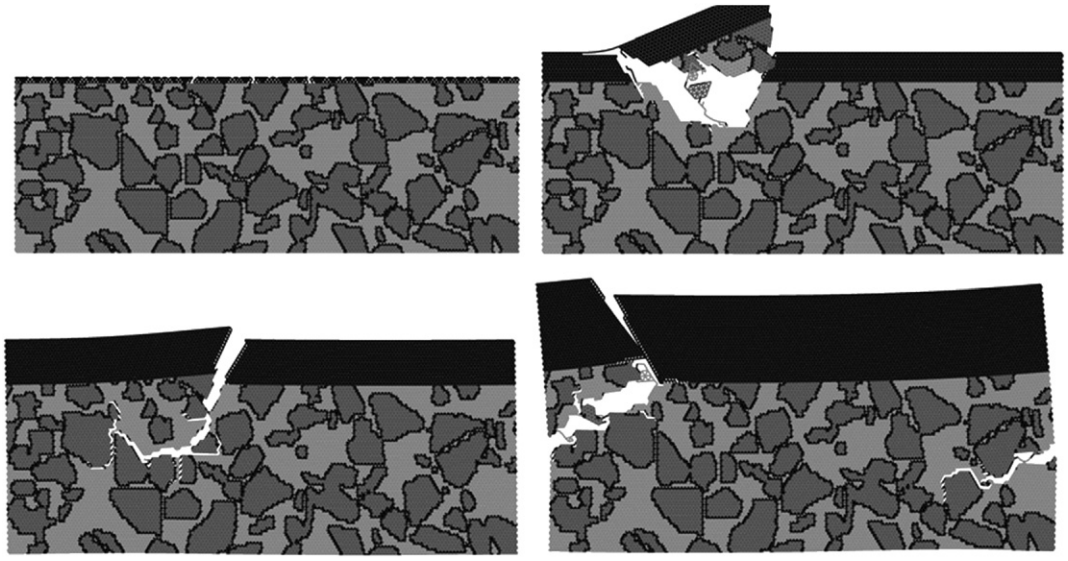

Fig. 12. Effect of ice-layer thickness (1, 3, 5 and 10 mm) on the FSS damage magnitude.

show the effect of ice thickness rather than to demonstrate a realistic FSS for the condition given in Table 3.

In Fig. 12, the effect of various ice-layer thicknesses on the FSS of the identical mortar specimens is shown. The results imply that the new numerical model is able to simulate the experimental observations. Indeed according to the model, increasing depth of ice results in more severe surface damage under frost salt attack.

It might be noteworthy to mention that no damage is observed for 1 mm ice thickness of ice in the modeling results. This is – as mentioned before – simply because of a mismatch between the micromechanical properties of the specimens used in the experimental study and the ones used in the numerical modeling. It is quite possible that the micromechanical values used in the model for matrix and interfacial zones were different than that of real condition. Another reason could be that no real visco-elastic behavior for ice and mortar is implemented, but only a reduction of stresses is adopted. It should be noted that the pure ice cracks in the simulations because stress relaxation by creep is ignored.

The damage pattern created by the different thickness of ice could also be simulated by the model. The size of the scaled flakes in the experiments and the ones generated by the model are observed to be analogues for the corresponding ice thicknesses (see Fig. 6).

### *5.5. Modeling experimental parameters — external salt concentration*

Again the aim in this study was mainly to simulate the observations from the experimental study rather than achieving a numerical mass scaling result. In this modeling study the tensile strength of the interfacial transition zones were kept very low (0.1 MPa) in order to magnify the scaling damage and enable to differentiate the damage level easily. Another reason for keeping the tensile strength so low was to compensate the internal damage due to the ice formation [13] which is not included in this study.

The mechanical parameters of NaCl ice are different for various solute concentrations. Elastic modulus and tensile strength of the ice at different concentrations were estimated by the following equations provided by Valenza and Scherer [8];

$$\sigma_t(\mathrm{MPa}) = 2.47 - 5.15\sqrt{(1-\upsilon_i)} \tag{7}$$

$$E = E_i\left(\frac{\upsilon_i}{2.85 - 1.85\upsilon_i}\right) \tag{8}$$

where $\upsilon_i$ is the volume fraction of ice, $E_i$ is the elasticity modulus of pure ice, $E$ is the elasticity modulus of NaCl ice and $\sigma_t$ is the tensile strength of NaCl ice. The calculated mechanical values of NaCl ice having different salt concentrations are given in Table 5.

The numerical modeling results show that the new numerical model is able to simulate the experimental observations regarding the pessimum salt effect (see Fig. 13). According to the assumptions for the mechanical properties, 3% NaCl concentration creates maximum surface damage compared to the other solute concentrations. It was observed that at 1% salt concentration, generated stress was not able to crack the ice completely. Note that the deformations in the figure are not

Table 5
Mechanical properties of NaCl ice at −20 °C (as used in the model)

| Solute concentration | Elasticity modulus (MPa) | Tensile strength (MPa) |
|---|---|---|
| 0% NaCl | 10,000 | 2.5 |
| 1% NaCl | 8460 | 1.21 |
| 3% NaCl | 6650 | 0.48 |
| 7% NaCl | 4160 | 0.05 |
| 12% NaCl | 2230 | 0.01 |

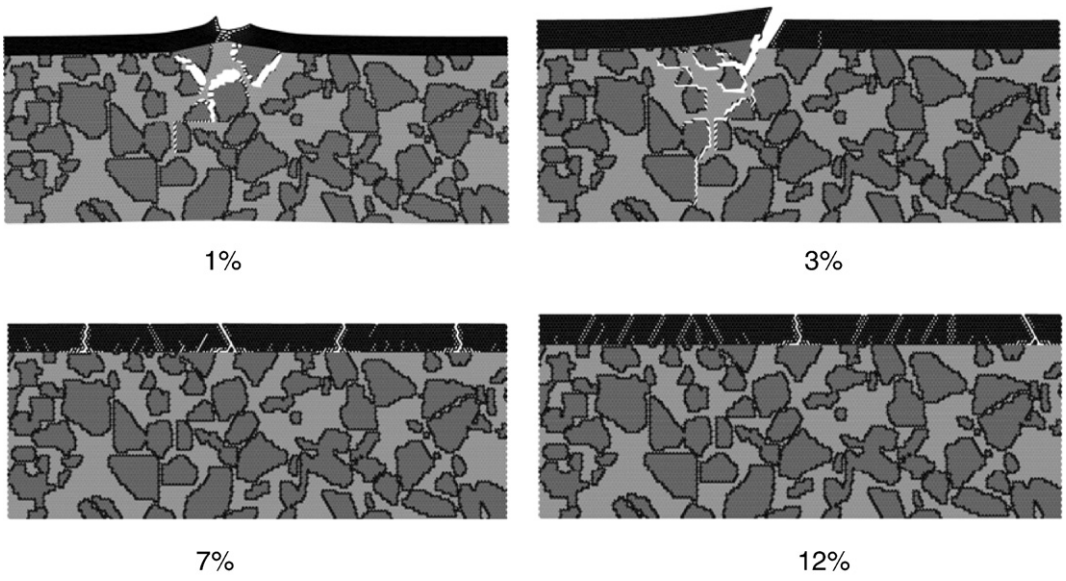


Fig. 13. Numerical modeling of the pessimum salt concentration effect on the FSS damage.

plotted at the same scale. Especially in the 1% case the deformations are exaggerated to be able to see the microcracks in the cement-based material. This caused an internal damage but this damage is not exactly a mass scaling as can be seen at 3% NaCl. In case of 7% and 12% NaCl solutions, the generated stress was just enough to crack the ice layer but not able to penetrate into the material skin.

## 6. Discussions

It appears that the new numerical model is able to simulate the FSS damage as well as the symptoms observed during the experimental study. The authors believe that the numerical model and *glue-spall* theory do fill a gap in understanding the FSS damage. However it should be strongly stressed that this model (and virtually any other model) has to be utilized with realistic ice and material microproperties in order to achieve realistic results. In this study the main aim was to evaluate the accuracy of the *glue-spall* theory and the validation of the new numerical model by the experimental findings. The model described in this paper certainly does not take all aspects into account. Earlier investigations suggested that chemical and thermodynamical issues do also affect the surface scaling [6,32,33]. Internal ice formation is also another important mechanism which has not been taken into consideration [2]. However, all those issues do have effect on the reduction of the material resistance against *glue-spall* action which tears-off the material skin. Therefore, the final resistance determines the level of damage rendered by external *glue-spall* action.

In the model, the analysis performed is linear elastic. It is assumed that the temperature drops to −20 °C and that the difference in thermal dilation between the material and the ice is $4\times10^{-5}$. In the analyses the crack in the ice starts at 22% of the linear elastic stress that is generated. This corresponds with the values described by Valenza and Scherer [8]. Due to the relaxation this will not be enough to crack pure ice, but probably will be enough to crack brine. The crack continues into the mortar and turns at a certain distance inside the material. Afterwards it continues until it hits the ice again, and a second crack in the ice is formed. Further continuation of the simulation would create another crack in the ice at another location, and the mechanism would repeat again. The mechanism is highly dependent on the choice of local material properties and relaxation of stresses. However, the nano-indentation technique seems to be an invaluable tool in approximating the real micromechanical values.

The modeling results clearly revealed that the FSS resistance of slag cement paste is significantly affected by carbonation. The cracks are observed to travel along the weak interstitial zones (PIS) between unreacted slag particles and the hydration products. On the other hand, non-carbonated slag cement paste showed no scaling because the microstructure was strong enough to confront the penetration of the cracks generated in the salt-ice.

In case of OPC paste, the non-carbonated microstructure showed significant surface scaling. This is because of the relatively weaker microstructure as found in the nano-indentation tests. Again the cracks traveled along the PIS and caused critical damage on the surface. It is interesting to see that carbonation is quite favorable for the OPC paste, presumably due to a resistant layer generated by the transformation of portlandite into calcite [34]. This reaction shows volume expansion which consequently reduces the capillary pore volume and enhances the micro-mechanical properties.

The study also suggests that the thickness of ice layer is extremely important to get consistent results. Although, the test standards prescribe the freezing liquid thickness, extra attention should be paid on this aspect during the experimental studies. Another important aspect which is related to this is the variation of the thickness within the ice layer. This variation is actually the surface roughness (or topography) of the cement-

based material being exposed and generally depends on the surface finishing method. This roughness determines the bond strength between ice and surface. Furthermore if the surface has a high roughness, additional peak stresses will be introduced in the ice that lead to a higher probability for the ice to crack, and thus a higher chance for scaling. Note that the roughness of the surface increases with increasing number of freezing–thawing cycles. Also surface cracking and ice formation inside these cracks will increase the scaling in every new freezing–thawing cycle [8].

The effect of ice-layer thickness during the FSS testing is generally prescribed by the standard test methods such as CDF, Scandinavian Slab Test and ASTM C672 [35–37]. In the CDF test, the specimen is soaked in the freezing salt solution and the specimens are exposed to 10 mm thickness of ice. In other tests, the thickness of freezing test liquid is prescribed as 3 mm and 6 mm for Scandinavian Slab Test and ASTM C672 respectively. As can be seen in the standards, there is no commonly used depth of salt solution. This brings the risk of having substantially different experimental results with different test methods. The authors believe that the thickness of the layer of ice in contact with the testing surface is extremely important, since thicker ice formation in contact with the material's surface would cause more mass scaling when the *glue-spall* action is the main mechanism. After the ice has cracked, the ice shrinks further and introduces stresses in the concrete. A thicker ice layer simply generates more force and thus higher stresses in the concrete surface, which should result in more scaling.

In general it can be concluded that:

- *if the thickness of the ice layer increases, the force that the ice exerts on the cement-based surface also increases, which results in more scaling;*
- *if the stiffness of the ice layer is higher, the force that the ice exerts on the cement-based surface increases, which results in more scaling.*

However, for the latter it has to be kept in mind that the strength of the ice should not be too high, since the ice can only exert stresses after it has cracked. This is the reason why pure ice generally does not lead to scaling for temperatures down to −20 °C. If the temperature will decrease further also pure ice will crack.

Therefore, it is also noteworthy that the lower the freezing temperature the higher the number of cracks generated in the materials surface [6]. This point needs to attract serious attention since all the major standard FSS tests specify the minimum temperature at −20 °C. This value might be reasonable for the climates in Norway or Canada but seems to be quite harsh for the regions having moderate winters such as The Netherlands where the minimum temperature hardly exceeds −10 °C. Hence, unfortunately the current specifications bring the risk of underestimation of the FSS durability of concrete mixture designs for the latter environmental conditions. The authors, therefore, suggest a revision in these standards to classify the climates and minimum temperatures accordingly.

## 7. Conclusions

A new FSS modeling is introduced based on Delft Lattice Model. The model can demonstrate the FSS damage in cement-based materials in accordance with previously proposed *glue-spall* theory: shrinkage of the ice layer which cools down further, cracks and introduces stresses in the material that lead to scaling.

Nano-indentation technique seems to be a very valuable tool for the estimation of micromechanical properties of the cement paste constituents to be modeled. A promising attempt has been presented in this paper concerning the FSS modeling of cement pastes. With the help of nano-indentation test results, it was possible to generate a model which behaves quite realistically under the frost and de-icing salt loading.

The study provided important insight regarding the dissimilar performance of slag cement and OPC pastes in carbonated conditions. It is concluded that carbonation is the key environmental parameter for the rich blended cement systems and in particular for systems rich in blast-furnace slag. There is important evidence that this is because of interstitial weak spaces with poor micromechanical properties created by the carbonation.

Experimental and modeling studies emphasize the necessity to revise minimum testing temperature in FSS tests. A revision could prevent underestimation of certain concrete mixtures to be used in mild climates *i.e.* in The Netherlands.

## Acknowledgements

The authors would like to thank Dr. George Scherer of Princeton University, U.S.A. and Dr. Wenzhong Zhu of the University of Pasiley, U.K. for their constructive discussions.

## References

[1] O. Copuroglu, Frost Salt Scaling of Cement-Based Materials with a High Slag Content, Delft University of Technology, The Netherlands, 2006, p. 188.
[2] M.J. Setzer, Micro-ice-lens formation in porous solid, Journal of Colloid and Interface Science 243 (2001) 193–201.
[3] T.C. Powers, The mechanisms of frost action in concrete, Stanton Walker Lecture Series on the Material Science, 1965.
[4] G.G. Litvan, Frost action in cement paste, Materials and Structures, 34, July–August 1973.
[5] M. Pigeon, R. Pleau, Durability of concrete in cold climates, Modern Concrete Technology, E&FN Spon, 1995.
[6] S. Lindmark, Mechanisms of Salt Frost Scaling of Portland Cement Bound Materials: Studies and Hypothesis, Lund University, Lund, Sweden, 1999, p. 266.
[7] M.T. Hasholt, Salt frost scaling — interaction of transport mechanisms and ice formation in concrete. PhD Thesis. 2002, Aalborg University.
[8] J.J. Valenza, G.W. Scherer, Mechanism for salt scaling of a cementitious surface, RILEM Spring Meeting 2004, RILEM Publishing, Chicago, USA, 2004.
[9] J.J. Valenza, G.W. Scherer, Mechanism for salt scaling, Journal of the American Ceramic Society 89 (2006) 1161–1179.
[10] W.C. Oliver, G.M. Pharr, Measurement of hardness and elastic modulus by instrumented indentation: advances in understanding and refinements to methodology, Journal of Materials Research 19 (2004) 3–20.
[11] W. Zhu, P.J.M. Bartos, Application of depth-sensing microindentation testing to study of interfacial transition zone in reinforced concrete, Cement and Concrete Research 30 (2000) 1299–1304.

[12] C. Fredericci, E.D. Zanotto, E.C. Ziemath, Crystallization mechanism and properties of a blast furnace slag glass, Journal of Non-Crystalline Solids 273 (2000) 64–75.
[13] G. Constantinides, F.-J. Ulm, The effect of two types of C–S–H on the elasticity of cement-based materials: results from nanoindentation and micromechanical modeling, Cement and Concrete Research 34 (2004) 67–80.
[14] K. Velez, S. Maximilien, D. Damidot, G. Fantozzi, F. Sorrentino, Determination by nanoindentation of elastic modulus and hardness of pure constituents of Portland cement clinker, Cement and Concrete Research 31 (2001) 555–561.
[15] J. Stark, H.-M. Ludwig, Freeze–thaw and freeze–deicing salt resistance of concretes containing cement rich in granulated blast furnace slag, ACI Materials Journal 94 (1997) 47–55.
[16] O. Copuroglu, A. Fraaij, J. Bijen, Microstructural change of blast furnace slag cement paste due to carbonation, vol. "Application of codes, design and regulations". Global Construction: Ultimate Concrete Opportunities, Thomas Telford publishing, Dundee, Scotland, 2005, pp. 229–234.
[17] O. Copuroglu, A. Fraaij, J. Bijen, C. Ladang, Pore characteristics of blast furnace slag cement systems, International Conference on Concrete and Reinforced Concrete, Moscow, Russian Federation, vol. 3, 2005, pp. 536–546.
[18] C. Li, A. Yoda, T. Yokomur, Pore structure, strength and carbonation of cement pastes containing ground granulated blast furnace slag, ACI Conference on Fly Ash, Silica Fume and Natural Pozzolans, SP 178–45, 1998.
[19] J.M. Chi, R. Huang, C.C. Yang, Effects of carbonation on mechanical properties and durability of concrete using accelerated testing method, Journal of Marine Science and Technology 10 (2002) 14–20.
[20] H.G. Smolczyk, Dauerhaftigkeit und porenstruktur von sehr alten betonen, Beton Informationen 26 (1986) 3–10.
[21] W. Manns, K. Wesche, Variation in strength of mortars made of different cements due to carbonation, The Fifth International Symposium on the Chemistry of Cement Tokyo, Japan vol. 3 (1968) 385–393.
[22] EN 196-1, Methods of Testing Cement — Part 1: Determination of Strength, 1995, p. 17.
[23] K.J. Verbeck, P. Klieger, Studies of salt scaling of concrete, Highway Research Bulletin 150 (1957).
[24] H.J. Herrmann, S. Roux (Eds.), Statistical Models for the Fracture of Disordered Media, Elsevier/North Holland, Amsterdam, 1990.
[25] E. Schlangen, J.G.M. van Mier, Experimental and numerical analysis of micromechanisms of fracture of cement-based composites, Cement & Concrete Composites 14 (1992) 105–118.
[26] E. Schlangen, E.J. Garboczi, Fracture simulations of concrete using lattice models: computational aspects, Engineering Fracture Mechanics 2/3 (57) (1997) 319–332.
[27] M. Jirásek, Z.P. Bažant, Macroscopic fracture characteristics of random particle systems, International Journal of Fracture 69 (1995) 201–228.
[28] J.E. Bolander, S. Saito, Fracture analysis using spring networks with random geometry, Engineering Fracture Mechanics 61 (1998) 569–591.
[29] R. Ince, A. Arslan, B.L. Karihaloo, Lattice modelling of size effect in concrete strength, Engineering Fracture Mechanics 70 (2003) 2307–2320.
[30] E. Schlangen, E.A.B. Koenders, K. van Breugel, Influence of internal dilation on the fracture behaviour of multiphase materials, Engineering Fracture Mechanics 74 (2007) 18–33.
[31] J. Stark, H.M. Ludwig, Freeze—deicing Salt resistance of concrete containing cement rich in slag, Frost Resistance of Concrete, E&FN Spon London, Essen, 1997, pp. 123–138.
[32] J. Stark, Frost resistance with and without deicing salt—a purely physical problem? Frost Resistance of Concrete, 1997, pp. 83–99.
[33] Y. Binbin, Durability of Reinforced Concrete in the Presence of Chloride Ions, Rijksuniversiteit Gent, Gent, 1988, p. 322.
[34] O. Wowra, Effects of carbonation to micro structure and pore solution, RILEM Workshop on Frost Resistance of Concrete, RILEM Publishing, Essen, Germany, 2002, pp. 61–68.
[35] CDF, Capillary suction of deicing solution and freeze thaw test, Materials and Structures 28 (1995) 175–182.
[36] SS137244, in 3rd Edition, Standardiseringkomissionen, Stockholm, Sweden.
[37] ASTM, C672-96 standard test method for scaling resistance of concrete surfaces exposed to deicing chemicals, Annual Book of ASTM Standards vol. 04.02 (1996).